Journal of Instrumentation

The Extreme Energy Events experiment: an overview of the telescopes performance.

To cite this article: M. Abbrescia *et al* 2018 *JINST* **13** P08026

Jinst

Published by IOP Publishing for Sissa Medialab

Received: *May 17, 2018*
Accepted: *August 21, 2018*
Published: *August 31, 2018*

The Extreme Energy Events experiment: an overview of the telescopes performance.

M. Abbrescia,[a,b] **C. Avanzini,**[a,c] **L. Baldini,**[a,c] **R. Baldini Ferroli,**[a,d] **G. Batignani,**[a,c] **M. Battaglieri,**[a,q] **S. Boi,**[a,e] **E. Bossini,**[a,o,e] **F. Carnesecchi,**[a,f] **A. Chiavassa,**[a,g] **C. Cicalo,**[a,h] **L. Cifarelli,**[a,f] **F. Coccetti,**[a] **E. Coccia,**[a,i] **A. Corvaglia,**[a,j] **D. De Gruttola,**[a,k,1] **S. De Pasquale,**[a,k] **F.L. Fabbri,**[a,d] **V. Frolov,**[p] **L. Galante,**[a,g] **P. Galeotti,**[a,g] **M. Garbini,**[a,f] **G. Gemme,**[a,q] **I. Gnesi,**[a,g] **S. Grazzi,**[a] **C. Gustavino,**[a,l] **D. Hatzifotiadou,**[a,f,o] **P. La Rocca,**[a,r] **G. Mandaglio,**[a,s] **O. Maragoto Rodriguez,**[n] **G. Maron,**[m] **M.N. Mazziotta,**[a,t] **S. Miozzi,**[a,d] **R. Nania,**[a,f] **F. Noferini,**[a,f] **F. Nozzoli,**[a,u] **F. Palmonari,**[a,f] **M. Panareo,**[a,j] **M.P. Panetta,**[a,j] **R. Paoletti,**[a,e] **W. Park,**[n] **C. Pellegrino,**[m] **L. Perasso,**[a,q] **F. Pilo,**[a,c] **G. Piragino,**[a,g] **S. Pisano,**[a,d] **F. Riggi,**[a,r] **G.C. Righini,**[a] **C. Ripoli,**[a,k] **M. Rizzi,**[a,b] **G. Sartorelli,**[a,f] **E. Scapparone,**[a,f] **M. Schioppa,**[a,v] **A. Scribano,**[a,c] **M. Selvi,**[a,f] **S. Serci,**[a,h] **S. Squarcia,**[a,q] **M. Taiuti,**[a,q] **G. Terreni,**[a,c] **A. Trifirò,**[a,w] **M. Trimarchi,**[a,w] **M.C. Vistoli,**[m] **L. Votano,**[a,l] **M.C.S. Williams,**[a,f,o] **L. Zheng,**[a,n,o] **A. Zichichi**[a,f,o] **and R. Zuyeuski**[a,n,o]

[a] *Museo Storico della Fisica e Centro Studi e Ricerche "Enrico Fermi", Roma, Italy*
[b] *INFN and Dipartimento Interateneo di Fisica, Università di Bari, Bari, Italy*
[c] *INFN and Dipartimento di Fisica, Università di Pisa, Pisa, Italy*
[d] *INFN, Laboratori Nazionali di Frascati, Frascati (RM), Italy*
[e] *INFN Gruppo Collegato di Siena and Dipartimento di Fisica, Università di Siena, Siena, Italy*
[f] *INFN and Dipartimento di Fisica e Astronomia, Università di Bologna, Bologna, Italy*
[g] *INFN and Dipartimento di Fisica, Università di Torino, Torino, Italy*
[h] *INFN and Dipartimento di Fisica, Università di Cagliari, Cagliari, Italy*
[i] *INFN and Dipartimento di Fisica, Università di Roma Tor Vergata, Roma, Italy*
[j] *INFN and Dipartimento di Matematica e Fisica, Università del Salento, Lecce, Italy*
[k] *INFN and Dipartimento di Fisica, Università di Salerno, Salerno, Italy*
[l] *INFN, Laboratori Nazionali del Gran Sasso, Assergi (AQ), Italy*
[m] *INFN CNAF, Bologna, Italy*
[n] *ICSC World Laboratory, Geneva, Switzerland*
[o] *CERN, Geneva, Switzerland*
[p] *JINR Joint Institute for Nuclear Research, Dubna, Russia*
[q] *INFN and Dipartimento di Fisica, Università di Genova, Genova, Italy*
[r] *INFN and Dipartimento di Fisica e Astronomia, Università di Catania, Catania, Italy*

[1]Corresponding author.

https://doi.org/10.1088/1748-0221/13/08/P08026

2018 JINST 13 P08026

[s] *INFN Sezione di Catania and Dipartimento di Scienze Chimiche, Biologiche, Farmaceutiche e Ambientali, Università di Messina, Messina, Italy*
[t] *INFN Sezione di Bari, Bari, Italy*
[u] *INFN and ASI Science Data Center, Roma, Italy*
[v] *INFN and Dipartimento di Fisica, Università della Calabria, Cosenza, Italy*
[w] *INFN Sezione di Catania and Dipartimento di Scienze Matematiche e Informatiche, Scienze Fisiche e Scienze della Terra, Università di Messina, Messina, Italy*

E-mail: daniele.de.gruttola@cern.ch

Abstract: The muon telescopes of the Extreme Energy Events (EEE) experiment are based on Multigap Resistive Plate Chambers (MRPC). The EEE network is composed, so far, of 53 telescopes, each made of three MRPC detectors; it is organized in clusters and single telescope stations distributed all over the Italian territory and installed in High Schools, covering an area larger than 3×10^5 km^2. The study of Extensive Air Showers (EAS), that is one of the goal of the project, requires excellent performance in terms of time and spatial resolution, efficiency, tracking capability and long term stability. The data from two recent coordinated data taking periods, named Run 2 and Run 3, have been used to measure these quantities and the results are here reported, together with a comparison with expectations and with the results from a beam test performed in 2006 at CERN.

Keywords: Particle tracking detectors; Performance of High Energy Physics Detectors; Resistive-plate chambers; Timing detectors

ArXiv ePrint: 1805.04177

2018 JINST 13 P08026

Contents

2018 JINST 13 P08026

1 Introduction

The Extreme Energy Events (EEE) experiment [1] is a project by Centro Fermi (Museo Storico della Fisica e Centro Studi e Ricerche "Enrico Fermi") [2], in collaboration with INFN (Istituto Nazionale di Fisica Nucleare), CERN (European Council for Nuclear Research) and MIUR (the Italian Ministry of Education, University and Research). EEE is designed to study Cosmic Rays (CR) and CR-related phenomena, via a synchronous sparse network of 53 tracking detectors spanning an area of more than 3×10^5 km^2, from Catania to CERN (with latitude from 37 to 46 degrees) and from Lecce to CERN (with longitude from 6 to 18 degrees). The map of the EEE array is visible in figure 1.

The EEE network is composed both by clusters and stand-alone stations; the result is a sparse network where each detection site is located at distances ranging from 15 m to several km from the one nearby. Each station (that defines a "telescope" for CR) is made of three Multigap Resistive Plate Chambers (MRPC), a CR dedicated version of the detector successfully used for Time Of Flight (TOF) systems and tracking detectors in high energy physics experiments at colliders (examples are the TOF system [4] of the ALICE experiment [5] at LHC and of the STAR experiment at RHIC [6]). Data collected by each station are sent to the CNAF center [7], the computing facility of the INFN, where they are stored, reconstructed and made available for analysis. The EEE network commenced

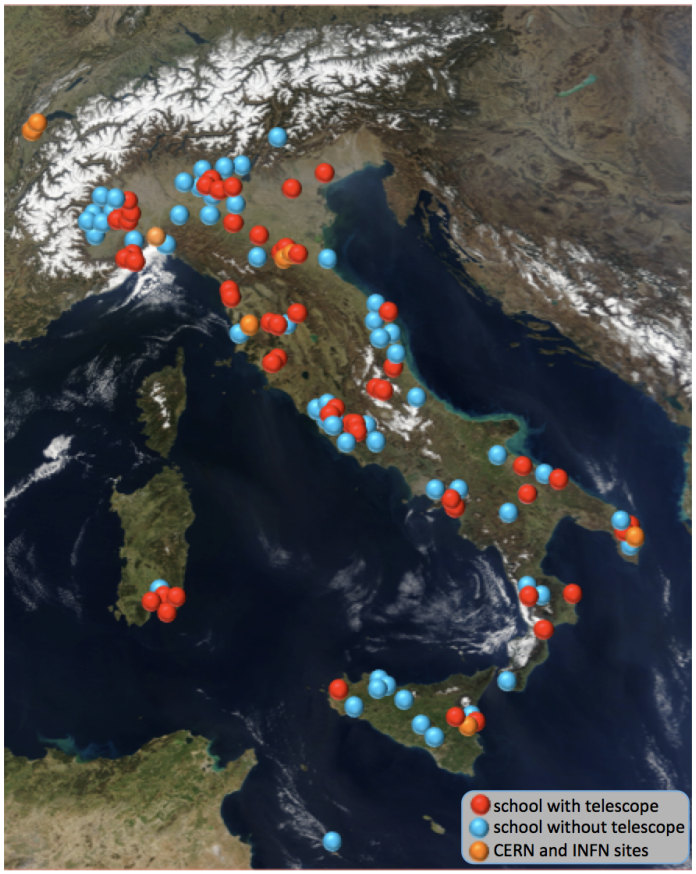

Figure 1. Map of the EEE array.

its operational activity in 2004 with a set of pilot sites in 7 Italian cities. In 2017 the observatory has grown up by a factor almost 8 in terms of number of telescopes. The EEE network is the largest and long-living MRPC-based system, with 53 sites instrumented and more than 12 years of data taking. The unconventional working sites, mainly school buildings with non-professional electrical lines, non-controlled environmental parameters and heterogeneous maintenance conditions, are a unique test field for checking the robustness, the ageing and the long-lasting performance of the MRPC technology for particle tracking and timing determination. In addition to the schools already hosting a telescope, 54 more institutes joined the project despite not being equipped with the detector; all the students contribute to the experiment by monitoring the telescopes performance and analyzing the available data. The students of all EEE schools perform a daily check of HV and current, gas flow, chambers multiplicity, event multiplicity and timing distributions. They operate the system if an intervention is required and in some cases they perform data analysis. Since 2014 the experiment started coordinated operation Runs (see table 1) and more than 50×10^9 muon tracks were collected up to June 2017 (end of RUN 3).

The topology of the EEE network allows to measure time-correlated events at distances never addressed before. Telescopes placed in the same city can detect individual EAS [8], whereas telescopes located hundreds of kilometers apart can detect the coincidence between two different correlated air showers, for which a few interesting events were found [9].

2018 JINST 13 P08026

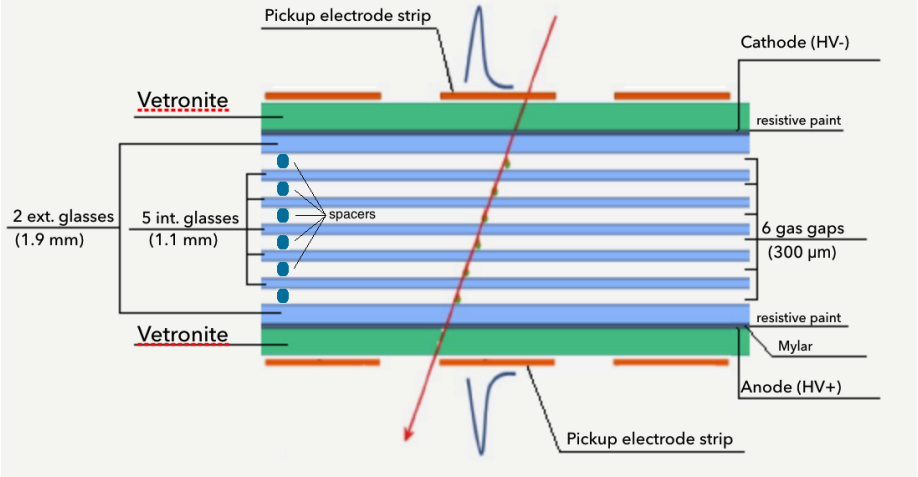

Figure 2. MRPC inner structure.

The EEE network can also address the local properties of the CR flux and its space weather-correlated features [10, 11], CR flux anisotropies in the sub-TeV energy region [12] and also phenomena related to the upward-going particle flux [13].

The EEE project has also a strong outreach impact: 47 detectors are installed in High Schools, where students and teachers actively participate to the data taking activities, taking care of the telescope operation and maintenance. Researchers coordinate and supervise activities, providing support during detectors construction, installation and operation. Students and teachers are introduced through seminars, lectures and master-classes, to the scientific research community, with the opportunity of understanding how a real experiment works, from the infrastructure development to the data acquisition, analysis and publications of scientific results.

2 MRPC for the EEE telescopes

The chambers composing the EEE telescopes are MRPC detectors specifically designed for combining good tracking and timing capabilities, low construction costs and easy assembly procedures [3]. Since the students of each participating school are directly involved in the construction of their own detectors, it is therefore important that the materials used are easy to find, safe and simple to assemble. The detector structure (figure 2) consists of 6 gas gaps obtained by stacking glass sheets, with voltage applied only to the external ones, and leaving the inner ones floating. The cathode and the anode consist of two glasses (160 cm × 85 cm, 1.9 mm thick) treated with resistive paint to build an electrode with a surface resistivity of 5–20 MΩ/□ that is connected to high voltage, the space between them being divided into the six narrow gaps (300 μm) by 5 intermediate glass sheets (158 cm × 82 cm, 1.1 mm thick); inner-glass spacing is assured through a weave made with fishing line. On the outer surfaces a sheet of Mylar (175 cm × 86 cm in dimensions) is stretched on a vetronite panel of equal area on whose external surface 24 copper strips are laid out (180 cm × 2.5 cm spaced by 7 mm), to collect the signals induced by particles. These 24 copper strips (i.e. cathode and anode readout strips) are mounted on both sides of the stack of glass plates, so that the signal (the sum of all gas avalanches in all the gaps) readout by one FEA channel is a differential signal

2018 JINST 13 P08026

of the cathode and anode strips. Two FEAs placed at the two edges of the chamber read the signal given by each strip. Two rigid composite honeycomb panels (180 cm × 90 cm) are used to assure good mechanical stability to the whole structure, which is enclosed in a gas-tight aluminum box (220 cm × 110 cm of external dimensions, 192 cm × 92 cm inside). A schematic top view of a chamber is shown in figure 3. The gas inlets and outlets, and the high voltage connectors are located at the ends of the longer sides, while the front-end (FEA) boards for the read-out of the strip signals are placed on the short sides.

Chambers are filled with a gas mixture consisting of a 98% / 2% mixture of R134a ($C_2F_4H_2$) and SF_6, at a continuous flow of 2 l/h and atmospheric pressure. The gas flow is provided by a commercial mixing system and it fills the chambers in daisy chain, with the exhaust connected outside. High voltage to the chambers is provided by a set of DC/DC converters, with output voltage roughly a factor 2000 with respect to the driving low voltage (LV). Stand-alone LV power supply units, both commercial or custom engineered by the EEE Collaboration, provide the LV to the DC-DC converters. The core unit of the DC-DC converters are the EMCO Q-series, both positive and negative, with a 10 kV full scale output. The HV stability declared by the manifacturer is ±10% at full load (50 µA). The typical working voltage of each DC-DC converter is from 8 to 9 kV, thus very close to the full scale. The total HV applied on the chambers is in the 18 to 20 kV range.

The aforementioned 24 copper strips that collect the signal, provide two-dimensional information when a cosmic muon crosses the chamber; in our reference system:

- the y coordinate is determined by the strip on which the signal is induced;
- the x coordinate is determined by measuring the difference between the arrival time of the signal at the two ends of the strip.

FEA cards (2 for each chamber) incorporate the ultrafast and low power NINO ASIC amplifier/discriminator specifically designed for MRPC operation [14]. Three MRPC chambers assembled in a telescope are shown in figure 4.

The trigger logic consists in a six-fold coincidence of the OR signals from the FEA cards (corresponding to a triple coincidence of both ends of the chambers), whose signals are combined in a VME custom made trigger module. The arrival times of the signals are measured using two commercial TDCs (CAEN V1190 — 64 and 128 ch — 100 ps bin). Synchronization between telescopes is guaranteed by a GPS unit that provides the event time stamp with precision of the order of 40 ns [15]. Data acquisition, monitoring and control are managed by a LabVIEW based program.

2.1 Track reconstruction, calibration and event selection

Data reconstruction is centrally managed at CNAF. Raw data are first processed to calibrate the telescope. Each readout channel has a time offset which slowly drifts in time, mainly in relation with environmental temperature variations. The drift is slow and does not affect a single run,[1] whose approximate duration is typically around half an hour. Every signal induced on a strip generates two time measurements, t_r or t, corresponding to arrival time of the signal to the edges of the chambers conventionally labelled as "right" and "left". The calibration is performed for each strip: the $t_{l_i} - t_{r_i}$ distribution of the i-th strip is used to calculate the mean value $\overline{t_{l_i} - t_{r_i}}$ for that strip. The mean is

[1] In this case run is meant as a data sample of 50k events, whose duration depends on the telescope rate.

2018 JINST 13 P08026

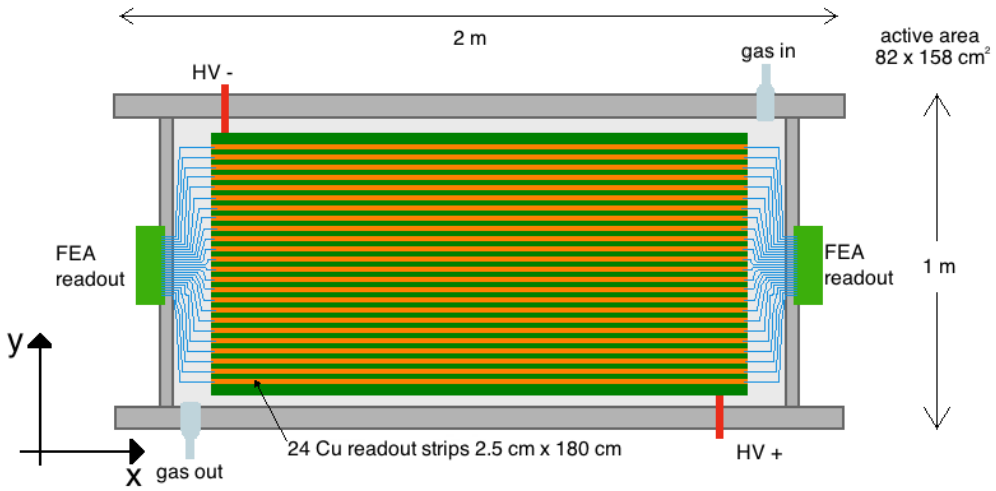

Figure 3. Top view of a MRPC chamber, showing the 24 copper strips, the 2 FEA at the edges of the chamber and the connectors where 2 DC/DC converters providing the HV (top left in blu and bottom right in red) are plugged in.

Figure 4. One EEE Project telescope located at Liceo Classico Massimo D'Azeglio in Turin, composed of three MRPC chambers.

2018 JINST 13 P08026

then subtracted to measurements $t_{l_i} - t_{r_i}$, so that the corrected mean value is set to zero. In this way all time differences on each chamber are equalized. Once the calibration is done, the corrected time values on one strip are paired to form a hit point.

As already pointed out, transversal coordinate is given by the strip number, while the longitudinal coordinate is given by the difference in the arrival time of the signal to the two chamber edges. A time value is also assigned to the hit, computed as the arithmetic mean of t_l and t_r and thus independent from the hit position. Cuts are then applied to exclude non physical hits by constraining their longitudinal position: the hit is rejected if t_l and t_r give an x coordinate larger than 79 cm on one of the two sides w.r.t. the center of the strip (i.e. we require the hit to be inside the active volume). After all hits are reconstructed, clusters are defined by grouping adjacent hits, if present. Hits (tagged 1 and 2) are clusterized if the following requirements are met:

- hits are on adjacent strips
- the differences $\Delta t_1 - \Delta t_2$, where $\Delta t_{1,2} = t_{l1,2} - t_{r1,2}$, is below 2 ns
- the hit time difference $t_{h1} - t_{h2}$, where $t_{h1,2} = \frac{t_{l1,2}+t_{r1,2}}{2}$, is below 2 ns

The time associated to the cluster is the smallest one. Finally, track reconstruction is performed. A linear fit of the clusters found in the three chambers is performed and the corresponding χ^2 is computed. All possible cluster combinations are used and ordered by their χ^2. The track candidates are defined by iteratively selecting the lowest χ^2 and removing the corresponding clusters, continuing up to the point when the whole set of available clusters has been assigned to a track. At the end a set of tracks with no hits in common is defined and transferred to the output file for analysis. The track selection for the measurements presented in this paper is done by requiring $\chi^2 < 5$ and rejecting events with more than 1 track. A χ^2 distribution before any cut is applied, for tracks collected by the EEE station labelled TORI-03, is shown in figure 5. Figure 6 shows the track multiplicity distribution for events with a $\chi^2 < 5$ before applying the multiplicity cut which is used only for the present performance studies.

Some interesting statistics from the four coordinated Runs taken so far are listed in table 1. Few considerations are due. The number of tracks w.r.t. the effective data taking period increased together with the number of telescopes included in the data taking. The slight decrease of the purity (candidate tracks/triggers) in Run 3 is due to the inclusion of few telescopes not yet optimized in Run 3 and well-performing in Run 4, that started in October 2017.

Table 1. Statistics from the four coordinated runs. The number of active telescopes in Pilot Run, Run 1, Run 2 and Run 3, is respectively 15, 28, 38 and 46. The purity is calculated as candidate tracks/triggers.

	Pilot Run	Run 1	Run 2	Run 3
starting date	27/10/2014	27/02/2015	07/11/2015	01/11/2016
ending date	14/11/2014	30/04/2015	20/05/2016	31/05/2017
number of days	19	63	196	212
tracks/day (M)	~ 27	~ 53	~ 69	~ 85
purity (%)	75	84	83	80

2018 JINST 13 P08026

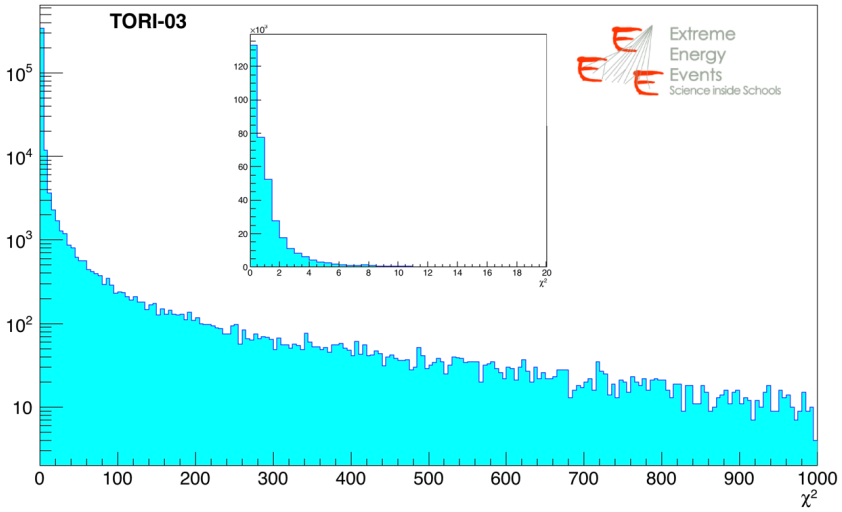

Figure 5. χ^2 distribution for one of the EEE telescopes (TORI-03, located in Piedmont) before any cut is applied. A zoom in the range $\chi^2 = [0, 20]$ is included.

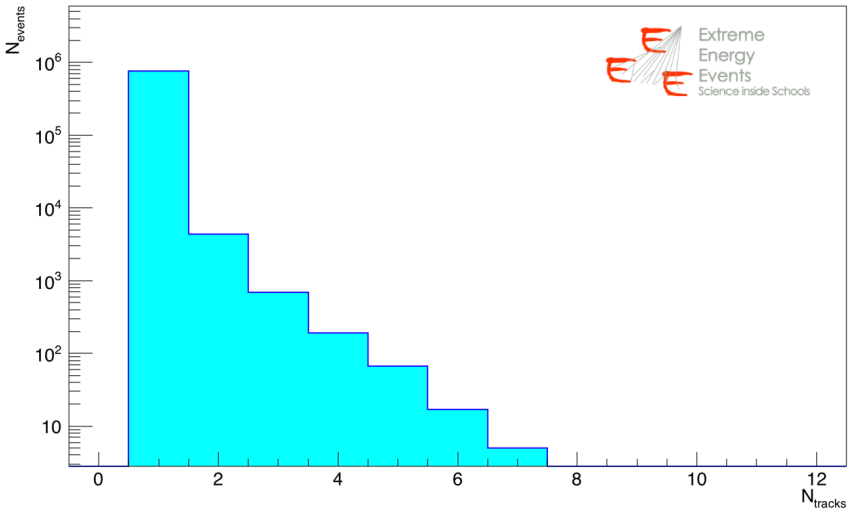

Figure 6. Track multiplicity distribution of one of the EEE telescopes (SALE-01, located in Campania); the applied cut is $\chi^2 < 5$ in this case.

The study of the detector performance (described in the next session) has been carried out by selecting a data sample from Run 2 and the recent Run 3. The whole EEE network has been used in the present analysis.

2018 JINST 13 P08026

3 Performance

In the next paragraphs the strategy to measure time and spatial resolution will be described. A sample of about 8×10^9 tracks over 31×10^9 collected during the Run 2 and Run 3 was used. Time resolution was derived analyzing a sample of events collected in Run 2 by telescopes TORI-03 (located in Piedmont) and PISA-01 (located in Tuscany). The main feature of the two telescopes is the fact that they were equipped with a dedicated board which distributed a common clock to the two TDC modules equipping each telescope. This prevented the slow shifts between the two internal TDCs clock, which could spoil the measured time resolution. In Run 3 the same clock distribution card was installed in all EEE telescopes allowing to assess the time resolution of all telescopes and compare the results with Run 2. A wider data sample from 44 telescopes has been used to evaluate spatial resolution. Telescope network time and spatial resolution results of the network are presented in paragraphs 3.1 and 3.2. Results of an efficiency measurement, performed without the need of an external detector are shown in paragraph 3.3. The last paragraph of this section (3.4) reports a study on the long term stability of the network, in terms of some quantities like tracking, multiplicity, trigger rate and time of flight.

3.1 Time resolution

The study of the time resolution σ_t has been performed by measuring the time information on the upper and lower chambers and using these values to determine the expected time on the middle chamber; this value is then compared with the hit time measured on the middle chamber. The width of the obtained distribution is proportional to the time resolution of the telescope. Time residuals used for the measurement of the time resolution are therefore defined as:

$$\Delta t = \frac{t_{\text{top}} + t_{\text{bot}}}{2} - t_{\text{mid}} \tag{3.1}$$

where t_{top}, t_{mid}, t_{bot} are the time values for single or clustered hits, as appropriate.

3.1.1 Results from RUN 2

The Δt distribution for TORI-03 (Run 2 data) is shown figure 7; the distribution is fitted with a gaussian function whose $\sigma_{\Delta t} = 269\,\text{ps}$. Assuming that the three chambers have similar timing performances, this implies a time resolution σ_t for the single chamber $\sigma_t = \sigma_{\Delta t}/\sqrt{\frac{3}{2}} = 221\,\text{ps}$. A similar analysis performed for PISA-01 gave a $\sigma_t = 270\,\text{ps}$ result. It is worth noting that the *time slewing* (TS) correction, explained in details in the next paragraph, is not applied in this case, while is included the analysis performed on Run 3.

3.1.2 Results from RUN 3

The readout electronics used in the EEE project [14] measures time using so-called *leading edge* discriminators (whose threshold can be chosen in a range from 0 to 1 V and was optimized by setting the value at 500 mV in all FEA) coupled to TDC. The time when the signal becomes lower than the threshold is instead called *trailing edge*. The Time Over Threshold (TOT) corresponds to the time difference between the times of the trailing and leading edges and is the time during which the signal remains over the threshold of the signal discriminator. The hit time depends on the signal

2018 JINST 13 P08026

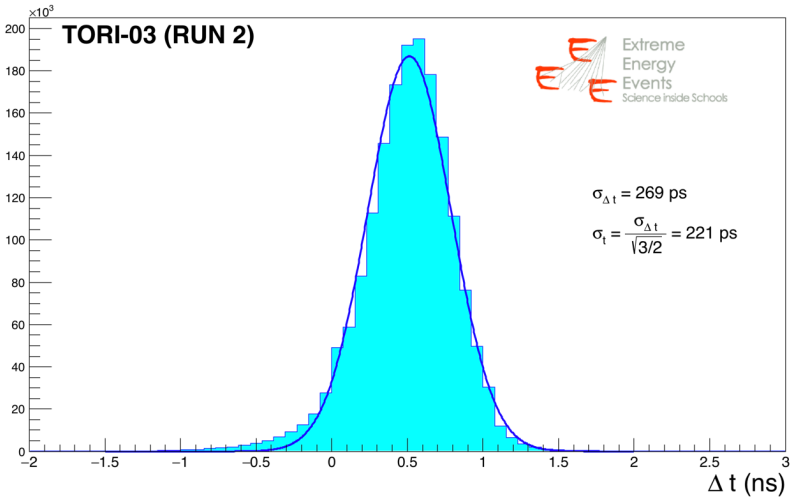

Figure 7. Δt distribution for one of the EEE telescopes (TORI-03), showing the gaussian fit and the time resolution $\sigma_t = 221$ ps. The data used in this case are from Run 2 and the *time slewing* (TS) correction is not applied. The displacement from zero of the mean values of the distributions are due to missing calibrations (i.e. z displacement of the middle chamber, cables length, electronics delay) and will be studied with RUN4 data.

amplitude, whose measure is roughly given by the TOT; its jitter can be corrected in order to extract the correct hit time (TS correction). The correction (performed on each chamber) makes use of the correlation between TOT and $t - t_{\text{exp}}$, the difference between the measured time t on a specific chamber and the time expected t_{exp} on the same chamber, determined by considering the other two chambers as reference. The procedure for TS correction is standard and can be found in [16]. An example of the mean time vs. TOT distribution for one chamber of one of the telescopes of the EEE network is shown in figure 8. Each point of this distribution represents the i-th mean value $t_{i,\text{TOT}}$ of the i-th bin of the profile histogram; these points are used to correct the measured time values t ($t_{\text{corr}} = t - t_{i,\text{TOT}}$). A linear interpolation is performed to get the mean value of $t - t_{\text{exp}}$ when TOT is between two bins.

Once the correction is determined, it is applied to each hit time and a new time distribution is built by using the corrected time t_{corr}, that can be used to measure the time resolution. Some examples are shown in figure 9, where the distributions before and after the TS correction are visible. The measurement has been performed on all the telescopes of the network and a $\approx 20\%$ improvement is obtained once the correction is applied. Depending on the telescope the time resolution ranges between 140 and 380 ps. The different values of time resolution for different telescopes can depend on three factors: missing optimization of the detector working point, possible inhomogeneities in MRPC construction, possible not optimal calibration for some strips. The first factor is also related to the dependence of the working point on pressure and temperature; the relative correction (see section 3.3.1) is not performed at the moment, but it will be done in Run 4. The other two factors should be less relevant, as the building procedure is robust and tests are periodically performed, as well as the calibration procedure. A distribution obtained with the values of time resolution from 33 telescopes of the network is shown in figure 10. A gaussian fit gives an average time resolution

2018 JINST 13 P08026

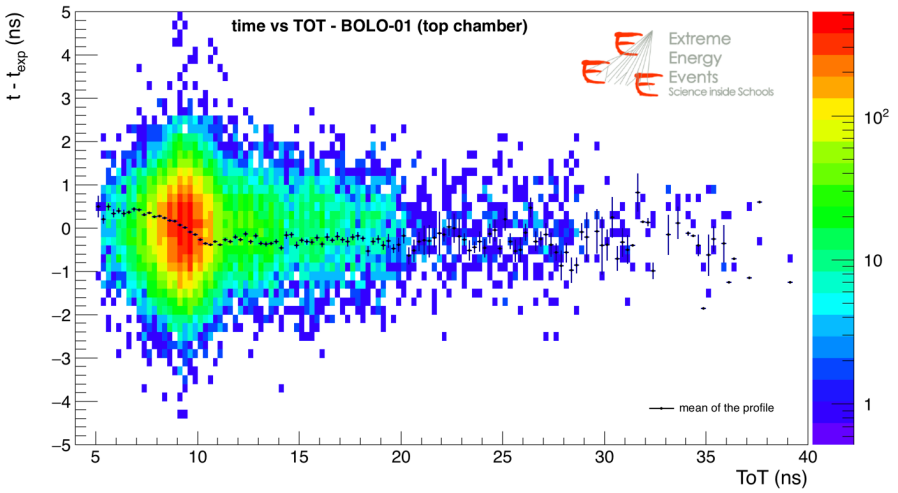

Figure 8. Correlation between TOT and the difference between the measured time and the time expected on the concerned chamber. The correction to be applied to each hit time is obtained from this distribution (for each single chamber). The distribution of one chamber of the telescope BOLO-01 (located in Emilia Romagna region) is shown here as an example.

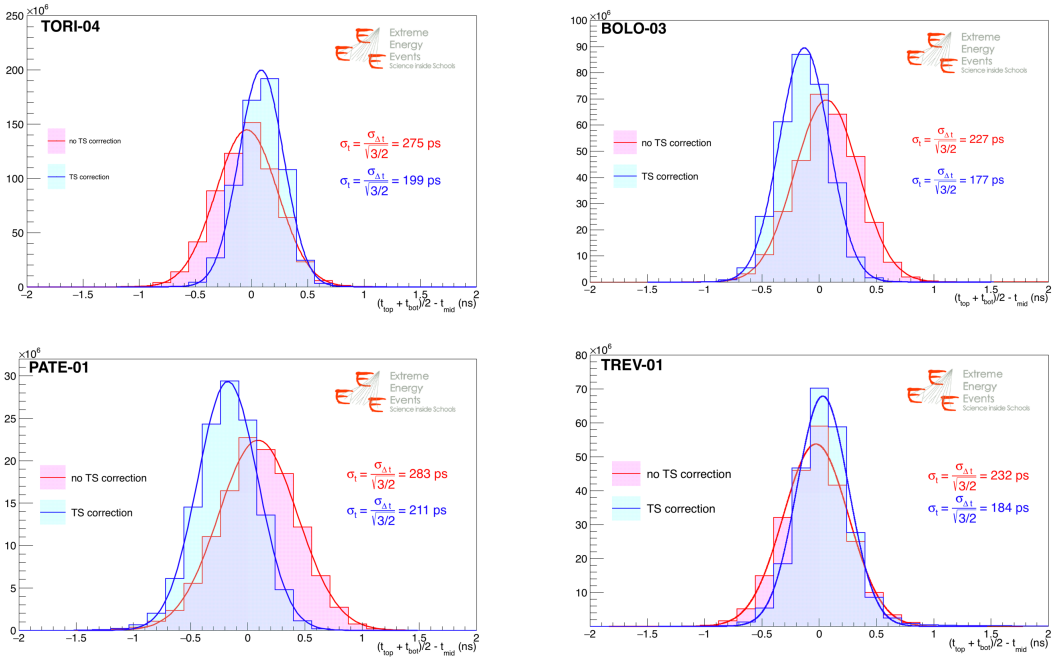

Figure 9. Time distributions for the telescopes: TORI-04, BOLO-03, PATE-01 and TREV-01 (respectively located in Piedmont, Emilia Romagna, Sicily and Veneto), measured with data taken in Run 3; the distribution and the time resolution before and after TS correction are shown. The displacement from zero of the mean values of the distributions are due to missing calibrations (i.e. z displacement of the middle chamber, cables length, electronics delay) and will be studied with RUN4 data.

2018 JINST 13 P08026

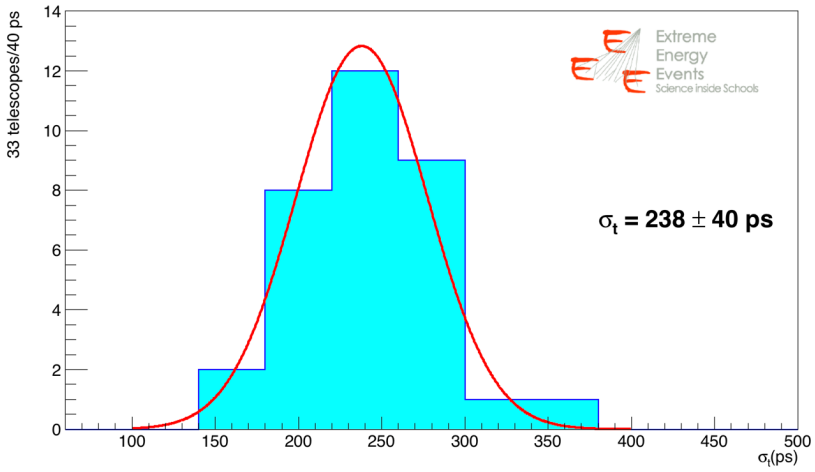

Figure 10. Time resolution measured with data taken in Run 3, for 33 telescopes; the average time resolution is given by the gaussian fit and is $\sigma_t = 238$ ps.

$\sigma_t = 238$ ps, with a sigma of 40 ps. This resolution is within expectations and totally compatible with Run 2 results and with EEE specifications. It can be compared with the value measured at the beam tests performed in 2006 at CERN [3] of 142 ps without TS correction and ≈100 ps with correction and t_0 subtraction; the smaller value is explained by the fact that at a beam-test conditions are well controlled, with a focused, monochromatic and collinear beam monitored with a set of MultiWire Proportional Chambers (MWPC) and scintillators. The working points optimization for the next data taking is expected to improve time resolution.

3.2 Spatial resolution

Spatial resolution is obtained by studying the distributions of the particle impact points in the three MRPC. It has been evaluated by measuring the spatial information on the upper and lower chambers and by using these values to determine the expected position on the middle chamber, both in the xz and yz planes (z being the coordinate orthogonal to the chamber plane). This value is then compared with the hit measured on the middle chamber. The residuals used to measure space resolution are therefore defined as:

$$\Delta x, y = \frac{x, y_{\text{top}} + x, y_{\text{bot}}}{2} - x, y_{\text{mid}} \tag{3.2}$$

Assuming the same space resolution in the three chambers, the space resolution along the strip (longitudinal resolution) of a single chamber can be calculated as $\sigma_x = \sigma_{\Delta x}/\sqrt{\frac{3}{2}}$ and along the short side (transverse resolution) as $\sigma_y = \sigma_{\Delta y}/\sqrt{\frac{3}{2}}$.

3.2.1 Longitudinal spatial resolution

The two signal arrival times, t_{right} and t_{left}, are related to the x_i coordinate of the hit, to the chamber length L and to the signal velocity along the strip v_{drift} by the following relation:

$$t_{\text{right}} = \left(\frac{L}{2} - x_i\right)\frac{1}{v_{\text{drift}}} \quad \text{and} \quad t_{\text{left}} = \left(\frac{L}{2} + x_i\right)\frac{1}{v_{\text{drift}}} \tag{3.3}$$

2018 JINST 13 P08026

Therefore the x position is evaluated as an average from both equations, by the difference of the two times:

$$x_i = \frac{t_{\text{left}} - t_{\text{right}}}{2} v_{\text{drift}} \tag{3.4}$$

where v_{drift} has been assumed[2] to be 15.8 cm/ns.

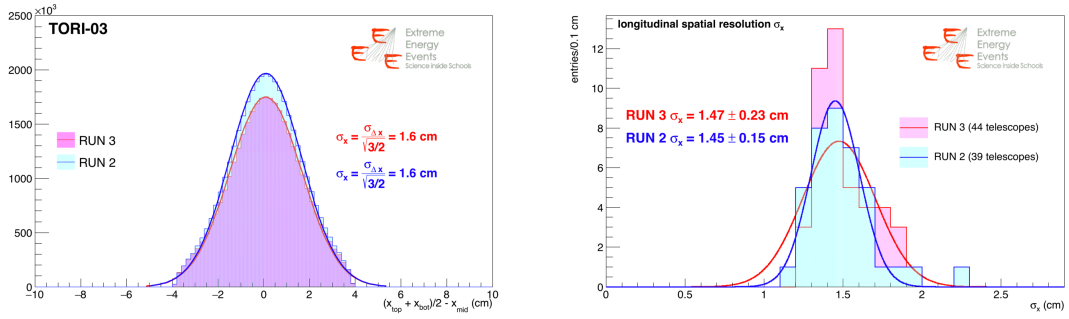

Figure 11. Left: example of longitudinal spatial resolution for one EEE telescope (TORI-03, located in Piedmont) in Run 2 and Run 3, obtained from a subsample of the data used for the whole analysis. Right: longitudinal spatial resolution measured with data taken in Run 2 (Run 3) for $n = 39$ (44) telescopes of the EEE network.

A sample of $2.7(3.5) \times 10^9$ candidate tracks collected in 30 days from 39 (44) telescopes in Run 2 (Run 3) has been used for this measurement. For each telescope the distribution Δx (see eq. (3.2)) has been plotted and used to derive σ_x, with the same strategy already applied to determine the time resolution; the distribution from TORI-03, obtained from a subsample of the data used for the whole analysis, is shown as an example in figure 11 (left). By fitting the distribution of the telescope residuals with a zero degree polynomial ($p_0 = 0.11 \pm 0.21$ in Run 2, $p_0 = 0.09 \pm 0.20$ in Run 3), the mean values are found to be compatible with zero for all telescopes, showing a good determination of the tracks direction. The comparison between the σ_x distributions from Run 2 and Run 3 are shown in figure 11 (right). The result from a gaussian fit gives an average longitudinal resolution of: $\sigma_{x_{\text{Run 2}}} = 1.4 \pm 0.1$ cm and $\sigma_{x_{\text{Run 3}}} = 1.5 \pm 0.2$ cm. The two results are in agreement, showing the stability of the network across the two runs. A comparable value has been measured before the network construction and published in 2007 in [17]. The longitudinal spatial resolution, measured at the beam test performed in 2006 at CERN previously mentioned, is 0.84 cm; the discrepancy with the measurement reported here is due to a set of missing uncertainty sources and different conditions w.r.t. beam tests (in a similar way as already explained in section 3.1.2).

3.2.2 Transverse spatial resolution

The expected transverse spatial resolution is derived considering the pitch of the strips (3.2 cm), $\sigma_{y_{\text{exp}}} \sim \text{pitch}/\sqrt{12} = 0.92$ cm.

The spatial resolution in the y direction was measured using the same data samples used to estimate the longitudinal resolution. For each telescope the distribution Δy (see eq. (3.2)) has been plotted and used to derive σ_y, applying the same strategy used for time resolution evaluation; the distribution from CAGL-02, obtained from a subsample of the data used for the whole analysis, is

[2] v_{drift} is derived by considering the length of the strip and the width of time distributions (10 ns).

2018 JINST 13 P08026

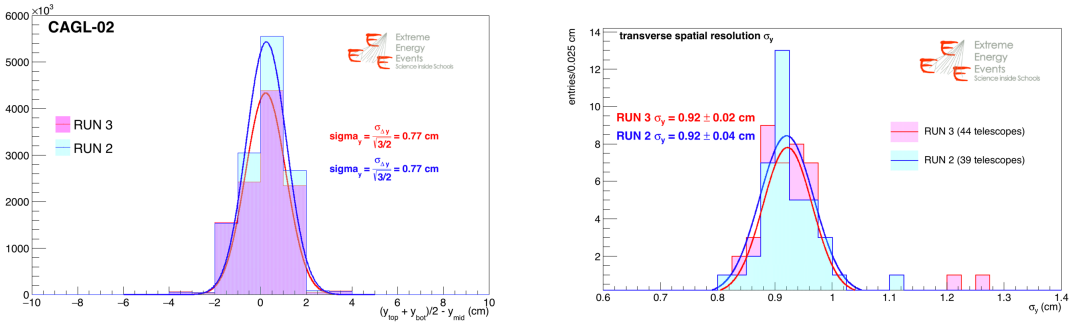

Figure 12. Left: example of transverse spatial resolution for one EEE telescope (CAGL-02, located in Sardinia) in Run 2 and Run 3, obtained from a subsample of the data used for the whole analysis. Right: transverse spatial resolution measured with data taken in Run 2 (Run 3) for $n = 39$ (44) telescopes of the EEE network.

shown as an example in figure 12 (left). Similarly to the longitudinal resolution, the mean values of the residuals in the transverse direction for all telescopes are compatible with zero ($p_0 = 0.04 \pm 0.14$ in Run 2, $p_0 = -0.01 \pm 0.14$ in Run 3). The distributions for Run 2 and Run 3 are reported in figure 12 (right). The average resolution is $\sigma_{y_{\text{Run 2}}} = 0.92 \pm 0.02$ cm and $\sigma_{y_{\text{Run 3}}} = 0.92 \pm 0.04$ cm, in very good agreement with the expectations.

3.3 Efficiency

Efficiency curves as a function of the applied voltage have been measured both at CERN, immediately after chamber construction, and after telescopes installation at schools; in most cases these curves have been obtained using scintillator detectors, employed as external trigger, and with additional electronics.

Later on, during data acquisition runs, the MRPC efficiency has been measured without using any additional detector, by using a slightly modified version of the reconstruction code. This method allows to check periodically the detectors performance and provides efficiency values, useful for all analysis.

3.3.1 Working point stability

The high voltage (HV) applied to an MRPC, or generally to a RPC-based detector, is a sensitive parameter for all applications involving absolute particle flux measurements or relative measurements performed over a long time period. The working point of the detector is ideally fixed within the efficiency *plateau* region, 300-400 V beyond the knee of the efficiency curve and at the lowest allowed value, in order to limit the chamber spurious counting rate, which usually ranges between 10 and 1000 kHz. There are two main sources inducing a fluctuation of the working point, with potential consequences on the efficiency: the environmental parameters and the DCDC converters stability.

Temperature and pressure are independent sources of instability for an RPC-based detector, as they affect the mean free path of the charges in the gas volume and thus the detector response [18]. To mitigate the variation, the EEE collaboration adopted two strategies. The temperature variations are reduced by conditioning the rooms where the telescopes are installed, while actions to fully stabilize

2018 JINST 13 P08026

the "effective" voltage HV_{eff} (eq. (3.5)), as described in [19], are under study. It is defined as:

$$HV_{eff} = HV \frac{p_0}{p} \frac{T}{T_0} \tag{3.5}$$

where standard pressure and temperature are set in our case to $p_0 = 1000$ mb and $T_0 = 298.15$ K.

The second source of HV fluctuation is related to the instability of the DCDC converters induced by temperature variations and internal drifts. The collaboration is therefore developing an automatic feedback system for the online stabilization of the HV_{eff}, acting directly on the applied HV to correct both the DCDC fluctuations and the effects of pressure and temperature. Any HV_{eff} fluctuation beyond 300-400 V (due for instance to changes in temperature and pressure) can move the working point of the chamber in the region left to the knee, where even a few tenths of Volts variation corresponds to a significant change in efficiency. An optimal choice of the working point of the EEE telescope is therefore fundamental to allow the EEE telescopes to be sensitive to phenomena involving a few percent particle flux variations, such as solar activity surveys and search for very rare events. Indeed since the EEE telescope trigger logic selects events detected by the three MRPC planes, the whole telescope efficiency is $\epsilon_{telescope} = \epsilon_t \times \epsilon_m \times \epsilon_b$, the product of the efficiencies of the top, middle and bottom chambers respectively. Therefore the identification of secondary muons flux variations is strongly affected by the single MRPC efficiency fluctuations. Assuming the three efficiencies being roughly equal to a common value ϵ, a small single chamber efficiency fluctuation $d\epsilon$ reflects in the telescope efficiency with a fluctuation (at the first order) $\approx 3\epsilon^2\, d\epsilon \approx 2.7\%$, in case of $\epsilon = 0.95$ and $d\epsilon \sim 1\%$. The typical flux variations connected to a Coronal Mass Ejection on the Sun span from 1–2% to 6–7%, thus setting the maximum allowed efficiency fluctuation to be well below 1%.

The searches for rare events are even more challenging. The detection efficiency of an EAS by a telescope cluster, composed by n telescopes, is $\epsilon_{cluster}$ proportional to ϵ^{3n}. The search for long distance correlations between EASs requires the coincidences between 2 clusters (at least 2 telescope each), setting the efficiency for such observations to $\epsilon_{cluster} = \epsilon^{12}$ (2 clusters made by 2 telescope each, 3 chambers per telescope). By considering $\epsilon = 0.95$ one obtains as the overall efficiency for these events $\approx 54\%$, applicable to the majority of the EAS events; the events with more than 1 tracks are a few per mille, being the surface of a EEE chamber roughly 1.3 m^2. However this estimation can be relaxed when studying events at higher track multiplicity.

These challenging measurements justify the efforts the collaboration is supporting to reach very stable HV_{eff} and applied HV.

3.3.2 Using the outer chambers as a trigger

The efficiency measurements, whose results are reported here, have been performed by changing from the standard 3-chambers operations to a 2-fold coincidence, excluding the chamber under test from the trigger. The two chambers in the trigger are also used for tracking and for selecting events with acceptable values of $1/\beta$ ($\beta = L/tc$, where L is the track length and t is the time of flight); in particular the $1/\beta$ distribution is fitted with a gaussian and events are accepted if the $1/\beta$ value is inside ± 0.7 from the mean value. Once a track is defined, the procedure requires to check if a hit is present on the chamber under test within a distance of 7 cm w.r.t. the expected (calculated) position. An HV scan of the chamber excluded from the trigger is performed, collecting about 150000 events

2018 JINST 13 P08026

per step. An example of the results of these measurements for the middle MPRC of 9 EEE telescopes is shown in figure 13. During the measurements atmospheric pressure p and temperature T were recorded, so efficiency is plotted vs. HV_{eff} (see eq. (3.5) in the previous paragraph). As shown in figure 13, all MRPC show a similar behavior, with efficiencies reaching almost 100% for an applied voltage larger than 18 kV.

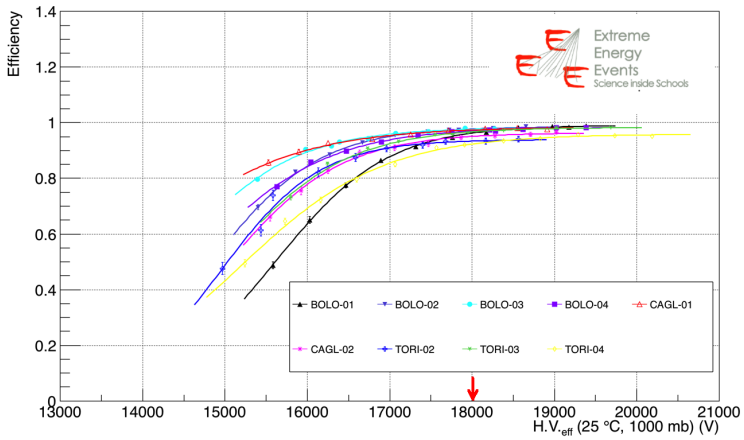

Figure 13. Efficiency vs. applied HV (corrected for standard p and T) of the middle MRPC of 9 EEE telescopes. The red arrow indicates the usual value chosen as working point.

This method was applied to the middle chamber of the EEE telescopes, but can be used to measure the efficiency of all the MRPC of a telescope by simply changing the trigger pattern, with the additional care of checking if the predicted hit position lies inside the fiducial area of the chamber under test. A distribution of efficiency values at the plateau from 31 telescopes (middle chamber) obtained from a three parameters sigmoid function [19] fit to each telescope efficiency curve is shown in figure 14. The fit parameters are the efficiency at plateau, the High Voltage at

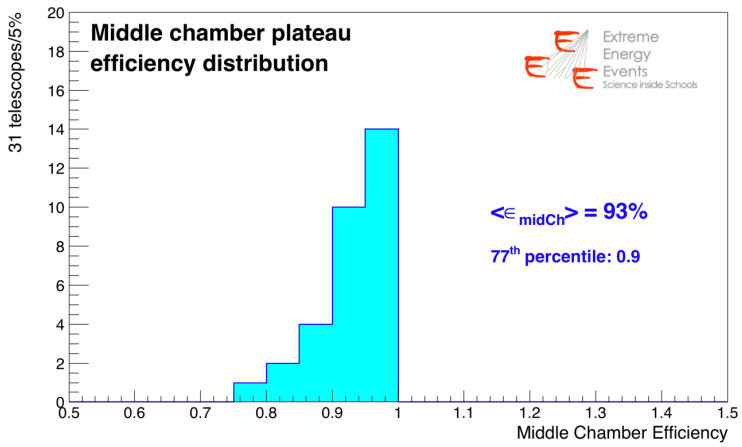

Figure 14. Distribution of the efficiency obtained at the plateau (corrected for standard p and T) of the middle MRPC for 31 EEE telescopes. An efficiency better than 90% is reached by 77% of the network.

2018 JINST 13 P08026

50% of plateau and the slope of the curve at flush. The average efficiency of the telescope network is around 93%, compatible with EEE specs and with results of the beam test performed in 2006 at CERN [3]. An efficiency better than 90% is reached by 77% of the network, corresponding to 24 telescopes out of 31. The cause of inefficiency for some telescopes can be related to dead strips and/or MRPC ageing.

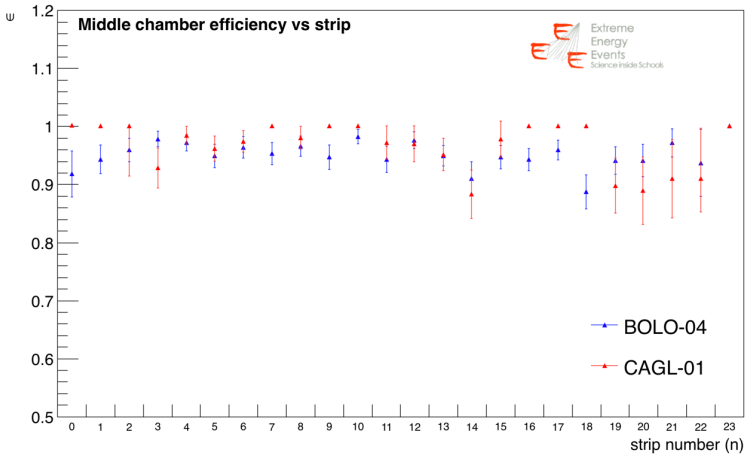

Figure 15. Efficiency vs. strip for 2 EEE telescopes (located in Emilia Romagna region and Sardinia).

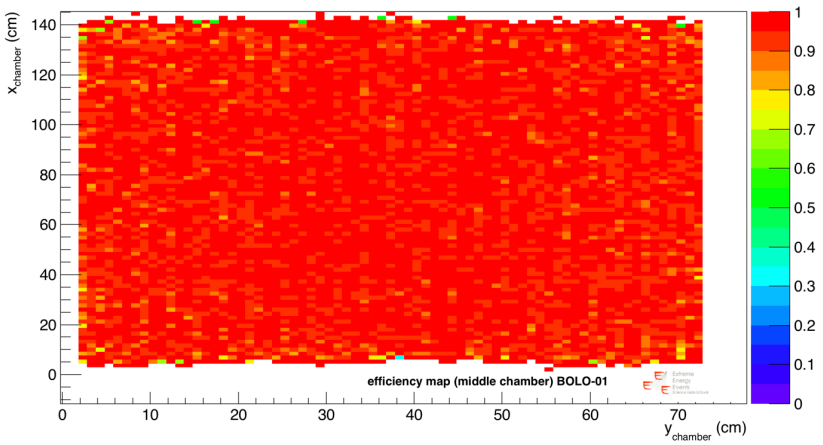

Figure 16. Efficiency map of BOLO-01 (located in Emilia Romagna region).

The efficiency strip by strip for two telescopes of the network, as an example, is shown in figure 15; the plot shows the efficiency spatial uniformity in the telescopes involved in this measurement. Possible lowering of the efficiency for some strips (taken into account in the reconstruction) are signaled thanks to this detailed measurement. Possible issues with the detector leading to low gain regions and/or non uniformity can be discovered by looking at the efficiency map; an example for one of the EEE chamber is shown in figure 16.

2018 JINST 13 P08026

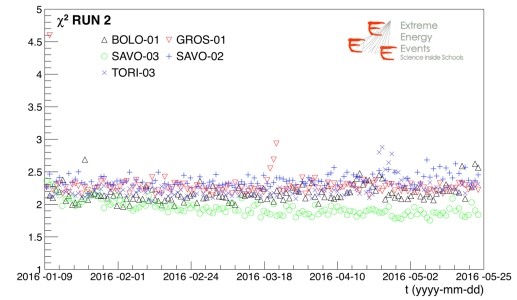

(a) χ^2

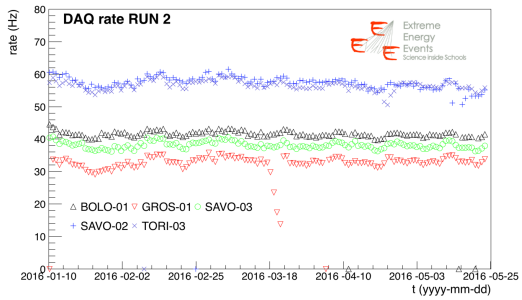

(b) DAQ rate

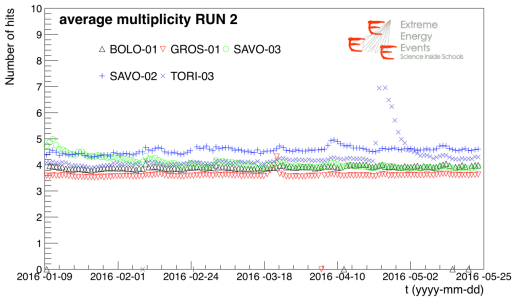

(c) Multiplicity

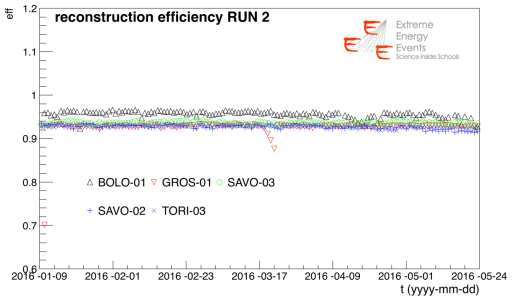

(d) Reconstruction efficiency

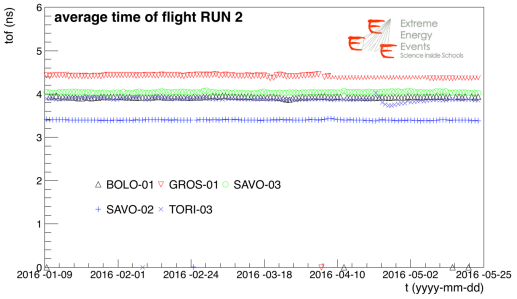

(e) Time of Flight

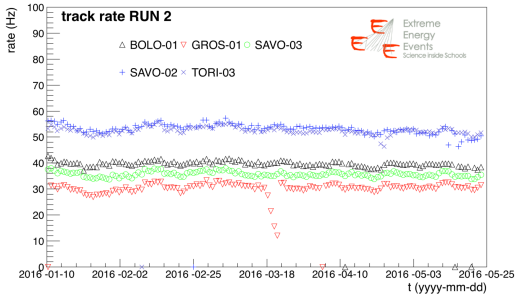

(f) Track rate

Figure 17. Run 2 trending plot for 5 EEE stations. Points at zero represent days when the telescope was not operational.

3.4 Long term stability

Long term performance stability is not easy to achieve with detectors hosted in schools, often far away from the nearest technical support. For telescope monitoring purposes an automatic Data Quality Monitor (DQM) has been created. For each file transferred to CNAF a set of parameters and rates are computed and published online. Daily report are also automatically generated, illustrating the evolution of the parameters over the last 48 hours. DQM allows for a fast reaction in case one station deviates from the standard behavior. Using the DQM and full reconstruction outputs, it is also possible to extend such trending plots to longer periods. As an example, trends for a selection of relevant quantities are reported in figure 17 for some telescopes of the EEE network:

2018 JINST 13 P08026

1. χ^2: average tracks χ^2;
2. *DAQ rate*: raw acquisition rate;
3. *Multiplicity*: average number of hits on the three chambers for each event;
4. *Reconstruction efficiency*: percentage of raw events where at least one track candidate has been found;
5. *Time of Flight*: average tracks TOF between top and bottom chambers;
6. *Track rate*: rate of events with at least one candidate track.

Data sample used in this case roughly covers 4.5 months of Run 2 for the five EEE telescopes with the best "live" time (time of active data taking). χ^2 and TOF together can be used to check the quality of the reconstructed tracks. Mean TOF values may be different for each station since distance between chambers are not the same for all installations. χ^2 is computed from the best (lowest χ^2) tracks in each event, if at least one hit on each chamber has been recorded. Note that these rates are sensitive to fluctuations in efficiency and noise rate of the detector, with the reconstruction efficiency used as cross-check. Hit multiplicity is a key parameter, because is extremely sensitive to gas and HV instabilities. Hit multiplicity is also available in the DQM for each chamber independently, and the average and the single chamber multiplicity for some of the telescopes of figure 17 are shown in figure 18. Deviations from the standard trending provides important warn-

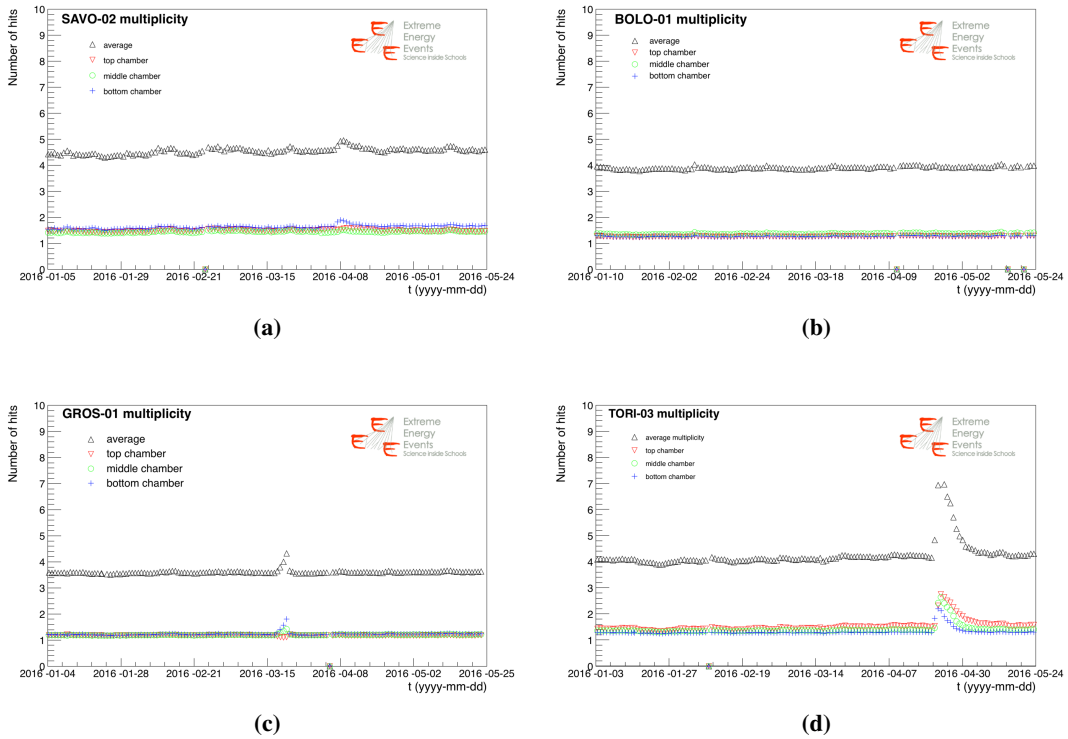

(a) **(b)**

(c) **(d)**

Figure 18. Average and per chamber hit multiplicity of SAVO-02, BOLO-01, GROS-01 and TORI-03 (located respectively in Liguria region, Emilia Romagna region, Tuscany and Piedmont); a sample from Run 2 data has been used.

2018 JINST 13 P08026

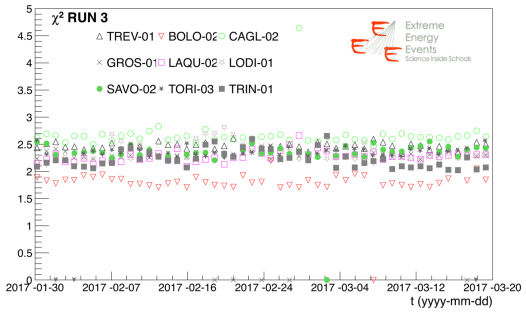

(a) χ^2

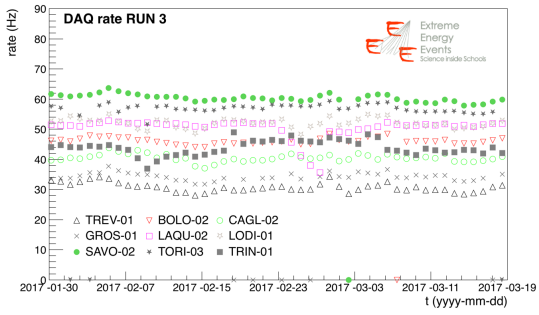

(b) DAQ rate

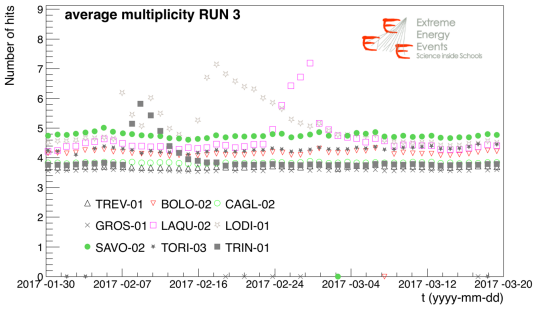

(c) Multiplicity

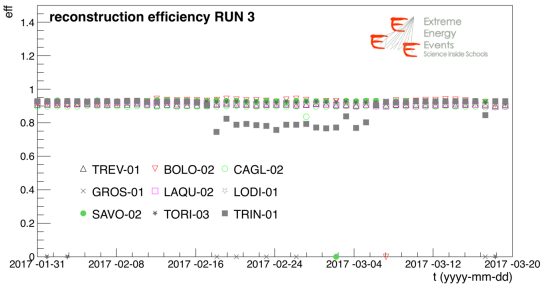

(d) Reconstruction efficiency

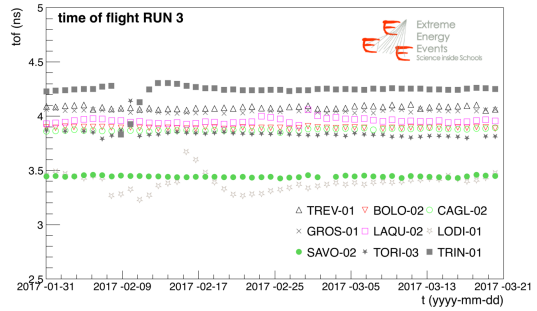

(e) Time of Flight

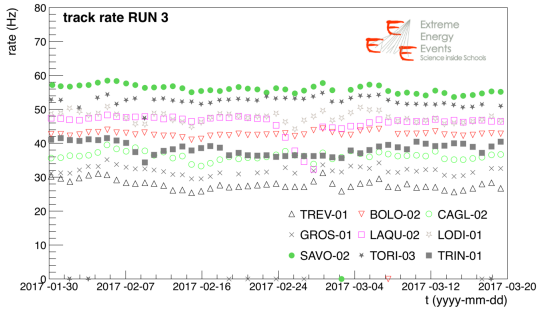

(f) Track rate

Figure 19. Run 3 trending plots for 9 stations. Points at zero represent days when the telescope was not operational.

2018 JINST 13 P08026

ings for the identification of problems and their solution. They might be due to cables not correctly plugged-in, malfunctioning of parts of the electronics, gas bottle exhausted. A long term stability study has been performed on 2 months out of Run 3 dataset and reported in figure 19, showing the same quantities of figure 17 for a subset of 9 stations. These plots are also useful to identify issues affecting a specific telescope for a limited period of time. For instance correlation between sudden multiplicity increases and drops in track reconstruction efficiency and track rate is clearly evident.

3.4.1 Future perspectives

The system presented will allow in the long term to study the ageing of the detectors and the impact on their performance. Considering the number of telescope available and the developed monitor software, the experiment here described will allow to study the long term ageing of the detectors and the impact on their performance. Although for most of the telescopes this study can be presently performed only in a time scale of few years, the current good quality of data from telescopes working since 2004 is an indication of a low impact of ageing.

4 Conclusions

The network of cosmic muon telescopes of the EEE Project, based on MRPC technology and covering about 10^6 km^2 across the Italian territory, has been successfully operated in the last years. More than 50×10^9 tracks have been collected by the network, during three data taking from 2014 to 2017. The observatory has grown up by a factor almost 8 in terms of number of telescopes w.r.t. 2007 and the EEE network is currently the largest and long-living MRPC-based telescopes network, with 53 active sites and more than 12 years of data taking. The unconventional working sites offer a unique check of the robustness, the ageing and the long-lasting performance of the MRPC technology for particle tracking and timing determination. The results of the analysis on the performance of the network are fully compatible with the EEE requirements in terms of efficiency ($\sim$ 93%), time resolution (238 ps) and spatial resolution (1.5 cm and 0.9 cm respectively for longitudinal and transverse direction). The good performance of the network allowed several analysis to be performed and published. Among them: search coincidences between near telescopes [8], study the muon flux decrease due solar events [10, 11], study of cosmic muon anisotropy at sub-TeV scale [12], study of muon decay into up-going events [13], search long distance correlations between EAS [9]. At the moment the EEE Collaboration is focusing on further improvements of the performance in terms of duty cycle and optimization of the working points of the telescopes.

References

[1] A. Zichichi, *Progetto "La Scienza nelle Scuole" - EEE: Extreme Energy Events*, Società Italiana di Fisica, Bologna (2004) [2nd edition, 2005; 3rd edition, 2012].

[2] http://www.centrofermi.it/EEE.

[3] M. Abbrescia et al., *Performance of a six gap MRPC built for large area coverage*, *Nucl. Instrum. Meth.* **A 593** (2008) 263.

[4] ALICE collaboration, *ALICE Time-Of Flight system (TOF): addendum to the Technical Design Report*, CERN-LHCC-2002-016.

[5] L. Cifarelli et al., *Insights from the ALICE quark-gluon coloured world at the LHC*, *Riv. Nuovo Cim.* **39** (2016) 497

[6] B. Bonner, H. Chen, G. Eppley, F. Geurts, J. Lamas Valverde, C. Li et al., *A single Time-of-Flight tray based on multigap resistive plate chambers for the STAR experiment at RHIC*, *Nucl. Instrum. Meth.* **A 508** (2003) 181.

[7] http://www.cnaf.infn.it/annual-report [ISSN 2283-5490].

2018 JINST 13 P08026

[8] M. Abbrescia et al., *First detection of extensive air showers with the EEE experiment*, *Nuovo Cim.* **B 125** (2010) 243.

[9] M. Abbrescia et al., *Search for long distance correlations between extensive air showers detected by the EEE network*, *Eur. Phys. J. Plus* **133** (2018) 34

[10] M. Abbrescia et al., *Observation of the February 2011 Forbush decrease by the EEE telescopes*, *Eur. Phys. J. Plus* **126** (2011) 61.

[11] M. Abbrescia et al., *The EEE experiment project: status and first physics results*, *Eur. Phys. J. Plus* **128** (2013) 62

[12] M. Abbrescia et al., *Looking at the sub-TeV sky with cosmic muons detected in the EEE MRPC telescopes*, *Eur. Phys. J. Plus* **130** (2015) 187.

[13] M. Abbrescia et al., *A study of upward going particles with the Extreme Energy Events telescopes*, *Nucl. Instrum. Meth.* **A 816** (2016) 142.

[14] F. Anghinolfi, P. Jarron, A.N. Martemyanov, E. Usenko, H. Wenninger, M.C.S. Williams et al., *NINO: An ultra-fast and low-power front-end amplifier/discriminator ASIC designed for the multigap resistive plate chamber*, *Nucl. Instrum. Meth.* **A 533** (2004) 183.

[15] A. Badalà et al., *Tests with GPS Camac Units for Educational Experiments on Cosmic Ray Physics*, INFN/TC-06/04, 17 February 2006.

[16] A.V. Akindinov et al., *Results from a large sample of MRPC-strip prototypes for the ALICE TOF detector*, *Nucl. Instrum. Meth.* **A 532** (2004) 611.

[17] S. An, D. Hatzifotiadou, J. Kim, M.C.S. Williams, A. Zichichi and R. Zuyeuski, *Cosmic ray tests of large area Multigap Resistive Plate Chambers*, *Nucl. Instrum. Meth.* **A 578** (2007) 139.

[18] M. Abbrescia, E. Bisceglie, G. Iaselli, S. Natali, G. Pugliese and F. Romano, *Resistive plate chambers performances at low pressure*, *Nucl. Instrum. Meth.* **A 394** (1997) 341.

[19] M. Abbrescia et al., *Cosmic ray tests of double-gap resistive plate chambers for the CMS experiment*, *Nucl. Instrum. Meth.* **A 550** (2005) 116.

2018 JINST 13 P08026